

RESEARCH ARTICLE

## Synergistic anticancer effect of silver nanoparticles and Measles virus vaccine strain against hormone-dependent and -independent breast cancer cells

Rajaa H. Salih<sup>1</sup>, and Wajeeh Obead Kachi<sup>2\*</sup>, Ahmed Majeed Al-Shammari<sup>3</sup>

<sup>1</sup> Mustansiriyah university, faculty of science, department, Baghdad, Iraq

<sup>2</sup> Middle Technical University, Institute of Medical Technology/ Al-Mansour, Iraq

<sup>3</sup> Experimental Therapy department, Iraqi Centre for Cancer and Medical Genetic Research, Mustansiriyah, Baghdad, Iraq

### ARTICLE INFO

#### Article History:

Received 24 September 2021

Accepted 28 November 2021

Published 01 January 2022

#### Keywords:

Measles Virus

Silver Nanoparticles

Combination Therapy

Cytotoxicity

Cell Lines

Anti-tumor

### ABSTRACT

**Objective(s):** This study aimed to prepare a stable colloidal silver nanoparticles (AgNPs) and assess its novelty combination therapy, which comprises AgNPs and lives attenuated Measles virus (MV) vaccine, to target breast cancer cells. The safety of the proposed therapy in normal breast epithelial cell lines (HBL-100) was evaluated.

**Methods:** Silver nanoparticles prepared by chemical reduction, The stability, size, and concentration of the colloidal component have been demonstrated by examining the ultraviolet-visible (UV-Vis) spectroscopy at various times using Zeta potential examination, atomic force microscopy (AFM), and atomic spectroscopy. MV was propagated using the VERO-hSLAM cell line. Cytotoxicity assay was evaluated on human breast cancer cell lines. The safety of the proposed therapy in normal Human breast Luminal epithelial cells was assessed to compare the effect against cancer cell lines.

**Results:** The formation of nanoparticles is confirmed by the appearance of a perfect surface plasmon resonance (SPR) band at 424 nm. The stability was proved via a slight change in the absorption intensity from 224 nm to 226 nm (immediately and after a month), respectively, and the value of the charge was -41.13 mV. NPs were spherical in shape and had an average diameter of 40.87 nm. The concentration was 13 µg/ml. The Chou–Talalay analysis revealed synergism between the Measles virus and silver nanoparticles in all tested cancer cell lines and there were highly significant differences (p-value<0.001) among them

**Conclusions:** The novel combination of AgNPs and MV showed effective antitumor activity against breast cancer cells with high safety in normal human breast cells.

### How to cite this article

Salih R.H., Kachi W., Al-Shammari A.M. Synergistic anticancer effect of silver nanoparticles and Measles virus vaccine strain against hormone-dependent and -independent breast cancer cells. *Nanomed Res J*, 2022; 7(1): 37-48. DOI: 10.22034/nmrj.2022.01.003

### INTRODUCTION

Breast cancer is the most prevalent adenocarcinoma worldwide and is considered one of the severe life-threatening diseases in women despite existing therapy methods, such as hormone therapy, radiotherapy, chemotherapy, and surgery(1). Breast cancer is difficult to treat, incurable, and requires unique active treatments. Several viruses, including the Measles

Virus (MV), vesicular stomatitis virus, vaccinia, herpes simplex virus, and reovirus, have been preclinically studied as oncolytic viral therapeutic agents with very promising results (2).

Cancer treatments are nonspecific to tumor cells, whereas virotherapy selectively capitalizes and destroys cancer cells with minimal damage to normal cells (3). Oncolytic viruses can infect cancer cells via membrane fusion or attachment to their receptors on the target cell's surface (4).

\* Corresponding Author Email: [wjeeh.kachi@mtu.edu.iq](mailto:wjeeh.kachi@mtu.edu.iq)

Live attenuated MV vaccine strains attracted much attention due to their ability to target diverse human tumors types (5).

**Measles Virus** vaccine strains have been used constantly in most human clinical trials. Combination treatment strategies, **such as chemotherapy, radiation, and nano therapy treatments, were used to deliver good opportunities** to eliminate tumors. Recently, nanomedicine has played a key role in diagnosing and treating types of cancers, such as liver cancer; nanoparticles are considered one of the new agents that can produce promising results in targeting tumor cells. Many nanomaterials **were** used for medical and biological applications, especially in tumors, due to the tumor's acidic environment characteristic, **which** has a **direct** relationship with the nanoparticles (6).

Nanoparticles are characterized via their selectivity, charge, shape, density, and particle size and provide new solutions **to diagnose and treat various cancer diseases with properties of minimal effect on normal cells (7). silver nanoparticles (AgNPs)** have distinct chemical and physical properties, like size, character, size distribution, the outer part, and solubility, thus having great therapeutic potential. Different physical and biochemical approaches **approved yielding** biocompatible nanoparticles with improved therapeutic properties (8). In general, one type of (AgNPs) fabrication approach is bottom-up procedures, such as chemical reduction (9). This method has been used to produce stable colloidal **silver nanoparticles (AgNPs)** by reducing silver ions by sodium citrate to produce a homogeneous preparation of mostly spherical silver particles that can remain stable for over a month. This method is one of the simplest and cheapest processes to obtain AgNPs (10).

In the current study, we combined the **Measles Virus** with **silver nanoparticles (AgNPs)** to increase the effectiveness against tumor cells while ensuring no toxicity on normal cells.

## MATERIALS AND METHODS

**Silver nitrate** ( $\text{AgNO}_3$ ) and Sodium citrate dihydrate ( $\text{C}_6\text{H}_5\text{O}_7\text{Na}_3 \cdot 2\text{H}_2\text{O}$ ) were supplied by Sigma-Aldrich, USA. All the reagents were used as received, with no extra purification. We pretreated all glassware before use. The pretreatment procedure is as follows: first, the glassware was washed in a

blend of nitric acid and hydrochloric acid at a molar ratio of 1:3 half an hour and washed, then completed using **Double Distilled Water (DDW)** then sonicated for three minutes before discarded the water (this process was repeated thrice). Next, an oven was used to dry the glassware (1 h at 140 °C); afterward, it was treated with 3:1 sulfuric acid (95%) and hydrogen peroxide (30 wt.%) for 30 min; then, it was rinsed thrice in DDW in sonication for 3 min; lastly, the glassware was placed in the oven at 100 °C for one hour (11).

### *Silver nanoparticles (AgNPs) formulation*

Lee and Meisel's method was used to prepare silver colloids based on chemical reduction (12). High-level pure **silver nitrate** ( $\text{AgNO}_3$ ) and **Sodium citrate dihydrate** ( $\text{C}_6\text{H}_5\text{O}_7\text{Na}_3 \cdot 2\text{H}_2\text{O}$ ) (Sigma-Aldrich) were utilized without additional purification. Distilled water was used to prepare all solutions of reacting materials. Temperature and relative molar ratios of  $\text{Ag}^+/\text{cit}$  were considered the optimum parameters for the reaction. The stability of the optimal nanosuspension was obtained by varying these parameters until they were adjusted. In a typical experiment, the temperature was 96 °C–100 °C; the molarity of  $\text{AgNO}_3$  was constant, whereas the molarity of  $\text{C}_6\text{H}_5\text{O}_7\text{Na}_3 \cdot 2\text{H}_2\text{O}$  was changed; and the time of heating was 6 min. One-hundred milliliters of 1 mM  $\text{AgNO}_3$  was heated to boiling point, and 20 ml of 20.5 mM  $\text{C}_6\text{H}_5\text{O}_7\text{Na}_3 \cdot 2\text{H}_2\text{O}$  was added as a reducing agent. The solution was stirred vigorously with continuous heating. The colorless  $\text{AgNO}_3$  solution changed from pale yellow to ruby red and to dark brown; this change indicates the formation of AgNPs. After 6 min, the heating element was removed and the solution stirred until cooled to room temperature (13).

The equation below represents the mechanism of the reaction.

### *Characterization*

#### *Spectral investigation*

An ultraviolet-visible double-beam spectrophotometer (Cary-100 Conc, Australia) directly measured the AgNPs solution's absorbance spectra after production. Moreover, after one month, the absorbance spectrum of the same samples was measured to conform with the formation and stability of AgNPs in an aqueous solution (14).

#### *Zeta potential measurement*

A zeta nanosizer particle analyzer (Malvern, UK) was used to analyze colloidal AgNPs and determine the colloidal stability; the surface charge density of colloidal AgNPs that reflect stability must be measured.

#### *Atomic Force Microscopy (AFM) analysis of AgNPs*

The synthesized AgNPs were investigated using an AFM (Angstrom, AA3000, Advance Inc., USA) to determine the morphology, size, and particle distributions. The AFM images were acquired by placing a microvolume of the colloidal AgNPs solution onto high-grade mica and drying at room temperature in a clean laminar flow chamber.

#### *The concentration of the synthesized AgNPs*

The atomic spectroscopy model (AA-7000 SHIMADZU, Japan) was utilized to calculate the concentration of synthetic AgNPs at 328.1 nm.

#### *Cell lines*

Four cell lines, namely, **Michigan Cancer Foundation-7** (MCF-7), **breast cancer cell line (Centre Antoine Lacassagne-51)** (CAL-51), **Human breast Lumina-100** (HBL-100), and African green monkey kidney cell line (VERO-hSLAM), kindly provided by the experimental therapy department, the Iraqi Center for Cancer and Medical Genetics Research, Mustansiriyah University. All cell lines were cultured and maintained in minimum essential medium (MEM) with two mM L-glutamine, **4-(2-hydroxyethyl)-1-piperazineethanesulfonic acid** (HEPES), penicillin/gentamycin 100 µg/mL, and fetal calf serum 10% (US Biological, USA) in standard growth features (5% CO<sub>2</sub> at 37 °C).

#### *Virus*

Live attenuated MV vaccines (India) were dissolved with 5 ml of diluent supplied by the manufacturer. The virus was further passaged in VERO-hSLAM cells using serum-free MEM media. When the syncytia formation reached 80% to 90%, cells underwent three freezing and thawing cycles, and the virus was collected and stored.

#### *Titration of Measles Virus in cell culture*

The VERO-hSLAM cell line was inoculated in a 96-well plate (7000 cells/well in 50 µl). When the cell growth reached 80% after overnight incubation, a ten-fold dilution of the virus was

prepared. The virus was seeded in the plate at 50 µl/well as four wells for each dilution, whereas the control wells were inoculated with media. The microplate was left for one hour at 37 °C to facilitate virus adsorption. Two hundred microliters of the medium (1% serum) were added to each well after rinsing the cells with phosphate buffer saline (PBS) to remove the remnants of the nonassociated virus. The plate was covered with adhesive paper, incubated at 37 °C, and examined for 5 days to detect the **Cytopathic Effects** (CPE); MV titer was counted as defined by ((15)).

#### *Cytotoxicity*

The cytotoxic effect of synthesized AgNPs and MV was measured by using MTT solution (4,5-dimethylthiazol-2-yl-2,5-diphenyltetrazolium bromide) prepared as five mg per mL in PBS, pH 7.2 (Santa Cruz Biotechnology, USA). The MCF-7, CAL-51, and HBL-100 cells were cultured at 10<sup>4</sup> cells/well in 96-well flat-bottom microplates and incubated in a humidified incubator at 37 °C overnight. The cultured cells were exposed to AgNPs at a concentration of 0.40, 0.81, 1.62, 3.25, 6.5, and 13 µg/ml and to MV at a **Multiplicity Of Infection** (MOI) of 10, 6, 3, 1, 0.3, and 0.1, in addition, to control untreated cells as triplicate for each condition (16). The medium was discarded after 48h, MTT stain was added to the plate (100 µl/well) and incubated for two hours at 37 °C; afterward, 100 ml of dimethyl sulfoxide (DMSO) was added to each well before incubation for 40 min in the dark. A microplate reader was used to determine the absorbency at a wavelength of 492 nm. The cell growth inhibition rate counted, and the equation below was used to calculate cell growth inhibition (GI%).

$GI\% = \frac{a-b}{a} \times 100$ , where (a) is the OD of the control (mean), (b) is the OD of the test (17).

#### *Combination cytotoxicity assays and Chou-Talalay analysis*

MCF-7, CAL-51, and HBL-100 cell lines were distributed in flat plates (96-well) at 10000 cells/well and when the plates became confluent. At first, MV was added in different MOIs (10, 6, 3, 1, 0.3, 0.1) for one hour at room temperature. then, AgNPs were added at the indicated concentration (0.40, 0.81, 1.62, 3.25, 6.5, and 13 µg/ml). After 48h, MTT cytotoxicity assays were conducted to estimate the rate of growth inhibition; the assay was completed in triplicate. Median-effect doses

(ED50) were conducted for AgNPs and the MV for each cell line. For synergism purposes, the MV and AgNPs were calculated as inconstant proportions. To analyze the result of combination, CompuSyn software (ComboSyn Inc., Paramus, NJ, USA) was utilized to compute the Chou–Talalay combination indices (CIs) and variable ratios of MV and chemotherapeutics; moreover, alternately specific equations were used to conclude the CIs. A CI between 0.9 and 1.1 is considered additive, whereas a CI of 0.9 and 1.1 indicate synergism and antagonism, respectively.

## RESULTS

### UV/Vis spectroscopic analysis for studying the size distribution of nanoparticles

AgNPs were obtained through the reaction of silver ions as oxidizing agents with trisodium citrate dihydrate as reducing agents. The first noticed event was a color alteration. The color of the solution turned from pale yellow to reddish-brown at the end of the reaction (Fig. 1b). The UV-Vis spectra of colloidal AgNPs (Fig. 1a) demonstrated a perfect surface plasmon resonance (SPR) band at 424 nm. This peak confirmed the formation of AgNPs(18).

To obtain information about the stability of colloidal AgNPs, the spectra were documented immediately after preparation and after one month (without mixing and sonication). (Fig. 1a) (1) & (2) show that no substantial change occurred in the SPR band position or the spectral shape; the colloidal (AgNPs) absorption intensities changed slightly (224 nm to 226 nm). Moreover, this result shows that the synthesized AgNPs were stable at room temperature, with negligible aggregation for

1 month. Our results are consistent with those of (19).

### Zeta-potential of silver NPs

(Fig. 2) presents the zeta potential quantities of colloidal AgNPs. The value of the superficial charge was negative, that is,  $-41.13$  mV. High values were obtained, revealing remarkable stability. Thus, this silver fluid is ready for work.

### Atomic Force Microscopy analysis

The nanoparticles' shape and size are considered the main information obtained from AFM images (20).

(Figs. 3 and 4) present the AFM images and the size distribution histogram of AgNPs, respectively. The particles had a spherical shape and an average diameter of 40.87 nm. This value is consistent with previously reported values (21).

### The concentration of stock colloidal AgNPs

A 0.45  $\mu\text{m}$  Millipore filter-sterilized the colloidal AgNPs before measuring concentration, and they were analyzed by flame atomic absorption to determine the amount of Ag ions using the standard curve, which is displayed in (Fig. 5) The result was  $\sim 13$   $\mu\text{g/ml}$ .

### Synergistic anticancer effect of AgNPs and MV in MCF-7 and Cal-51 cancer cell lines

#### Cytotoxicity of the combined therapy on the MCF-7 cell line

**1. Ag NPs:** (Table 1, Fig. 6) show that AgNPs have a synergistic effect with MV on MCF-7 cells after an exposure period of (48 h) to all tested



Fig. 1. (a) UV-Vis's spectrum of synthesized silver nanoparticles (AgNPs) by reduction method. (1) Immediately after reaction termination. (2) After one month storage at room temperature): (b) Stages of color gradient during manufacturing

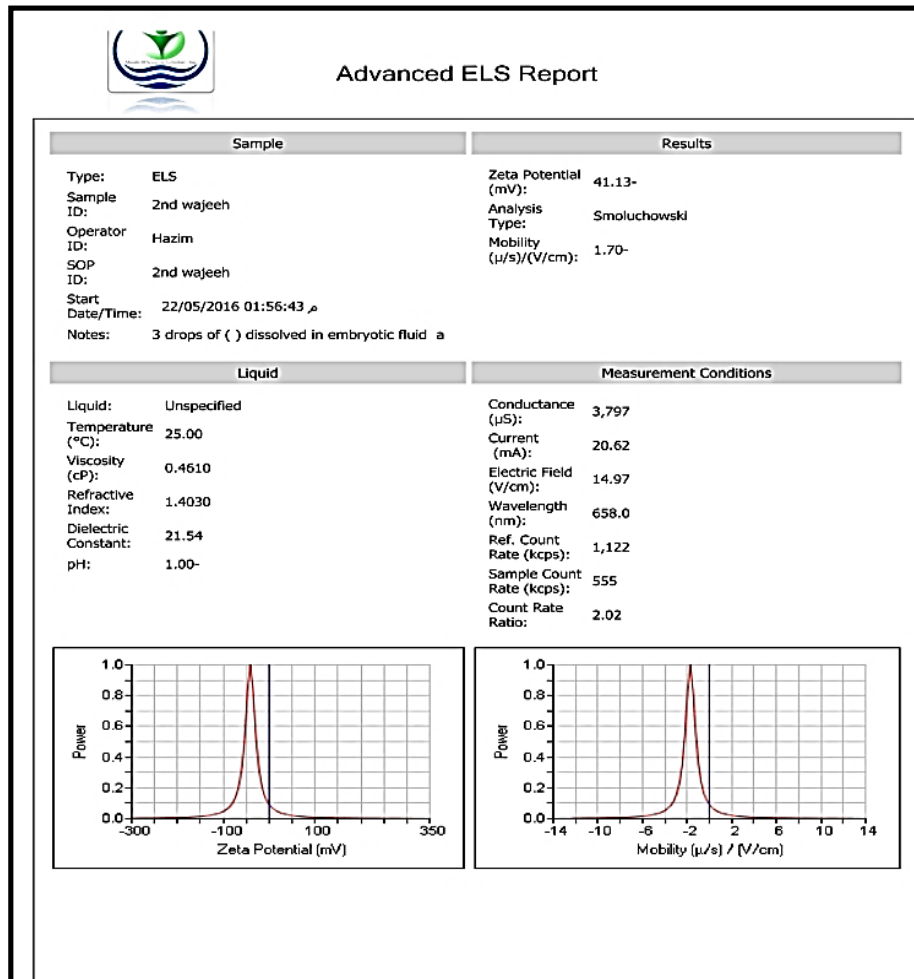


Fig. 2. Zeta potential analysis of synthesized silver nanoparticles (AgNPs) using chemical reduction method

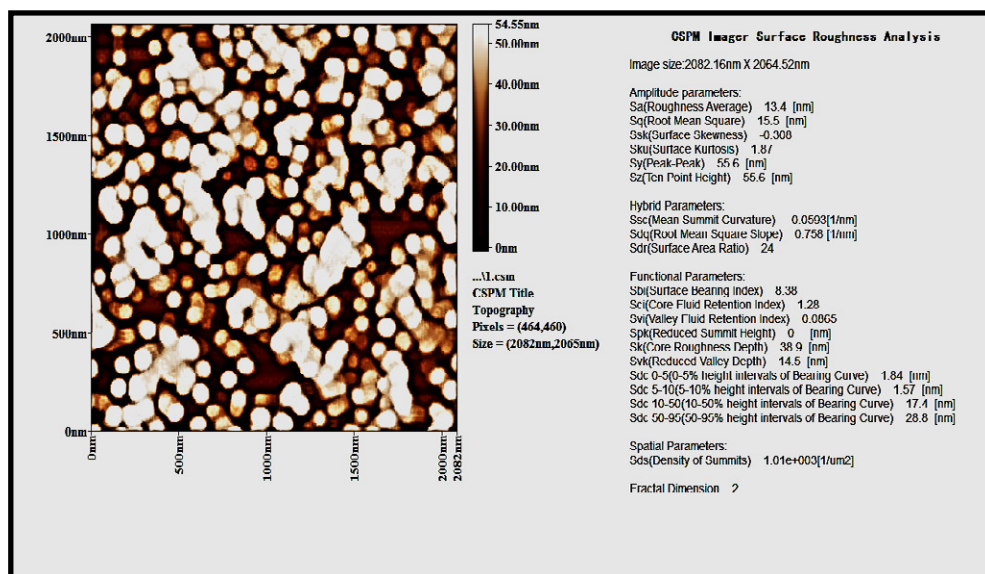


Fig. 3. Atomic Force Microscopy images of silver nanoparticles

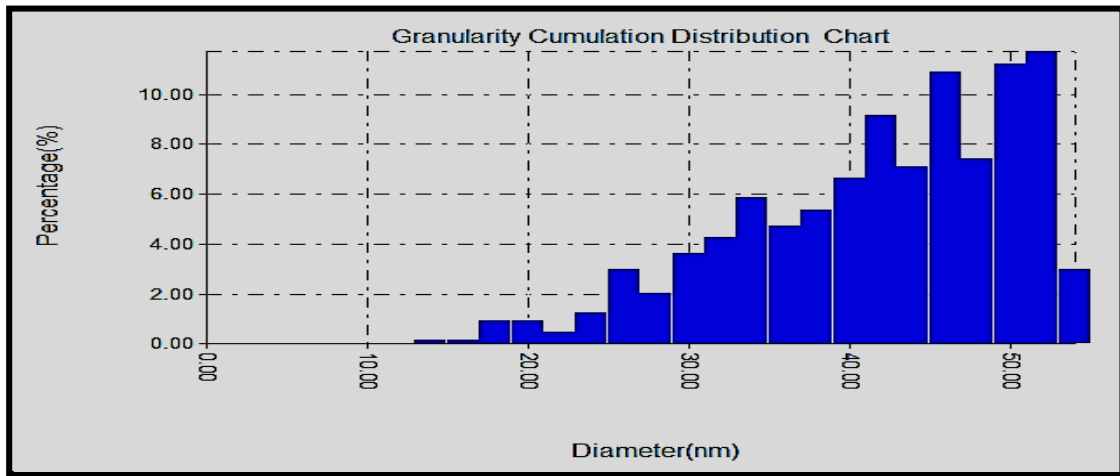


Fig. 4. size distribution histogram of silver NPs taken from the AFM images

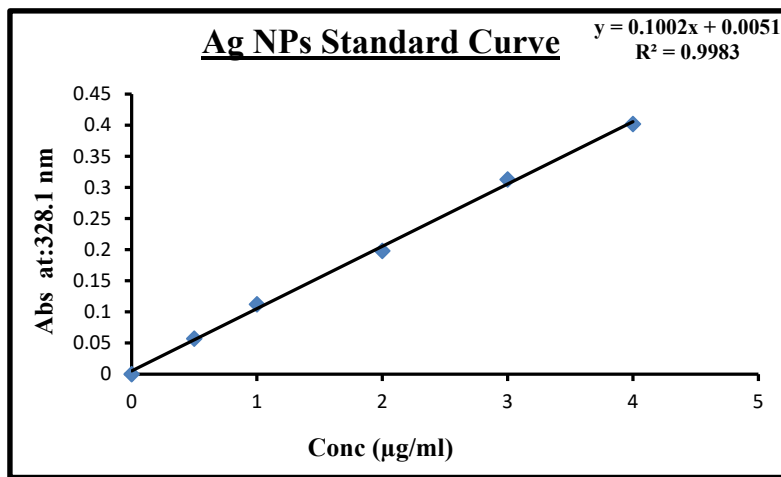


Fig. 5. Standard Curve of Flame Atomic Absorption for Ag ion

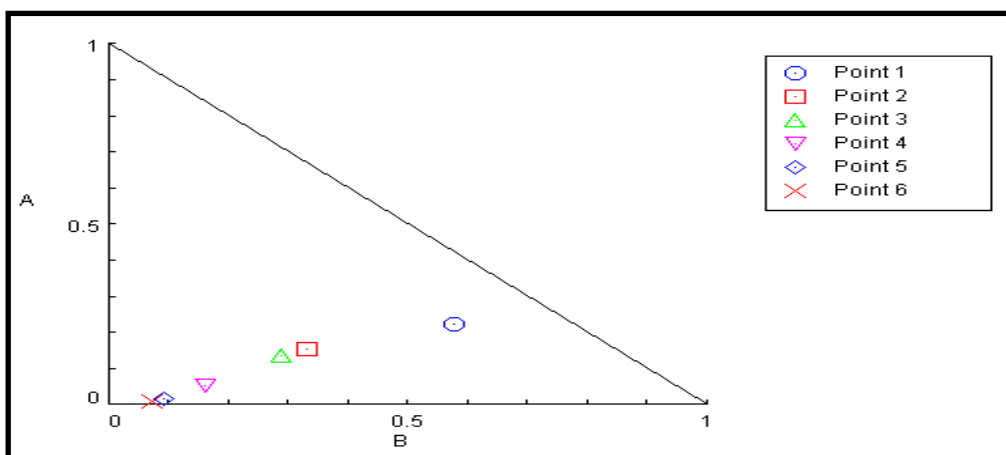


Fig. 6. Isobologram analysis showing the synergistic effect between MV and Ag NPs on MCF-7 cell line

Table 1. Synergistic effect of MV and AgNPs on the MCF-7 cell line

Point	MV(MOI)	Ag NPs (µg/ml)	G.I%	CI	Effect
1	10	13	0.77	0.79984	Synergism
2	6	6.5	0.76	0.48892	Synergism
3	3	3.25	0.72	0.42346	Synergism
4	1	1.62	0.71	0.21491	Synergism
5	0.3	0.81	0.70	0.11034	Synergism
6	0.1	0.40	0.66	0.08390	Synergism

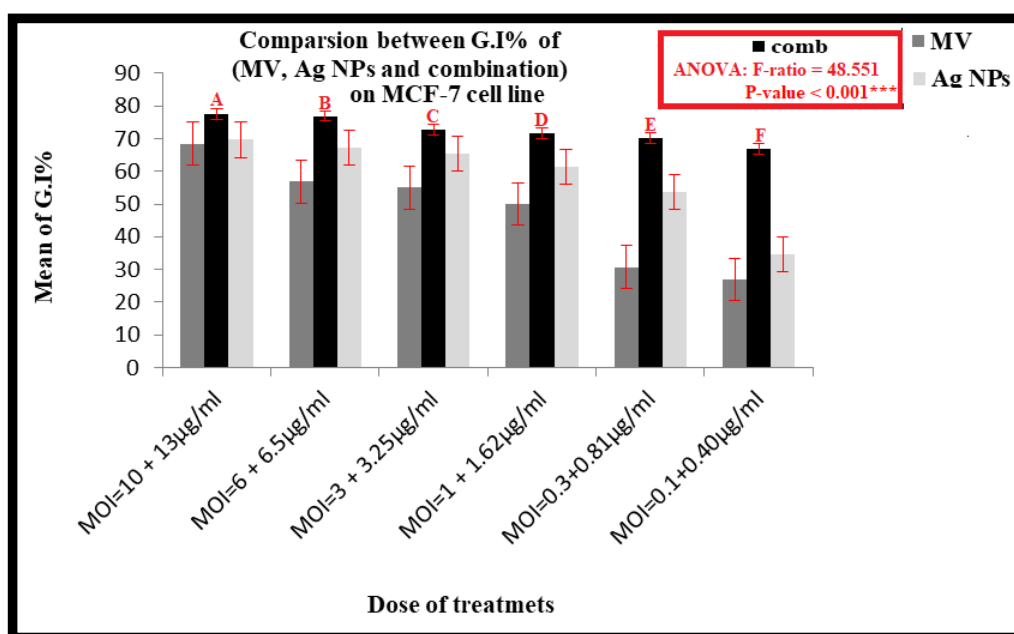


Fig. 7. Comparison between three treatments (MV, Ag NPs alone and MV+ Ag NPs) on MCF-7 cell line. According to Duncan's multiple range comparisons (DMRTs), the mean followed by different letters is significantly different. Means followed by the same letter are not significantly different

Table 2. Synergistic effect of MV and AgNPs on the Cal-51 cell line

Point	MV(MOI)	Ag NPs (µg/ml)	G.I%	CI	Effect
1	10	13	0.81	0.94645	Synergism
2	6	6.5	0.79	0.68269	Synergism
3	3	3.25	0.78	0.39119	Synergism
4	1	1.62	0.76	0.21669	Synergism
5	0.3	0.81	0.72	0.15350	Synergism
6	0.1	0.40	0.70	0.08873	Synergism

concentrations. (Fig.7) shows a comparison between all treatments (MV, AgNPs alone, and MV+AgNP combination) on MCF-7 cells **and the significant differences** at all six concentrations; the combination treatment has a higher growth inhibition rate than MV or AgNPs treatment alone.

*Cytotoxicity of the combined therapy on the Cal-51 cell line*

**1. Ag NPs:** (Table 2, Fig. 8) demonstrate that AgNPs have a synergistic effect with MV on Cal-51 cells after an exposure period of 48 h to all tested concentrations. **Moreover, there are significant**

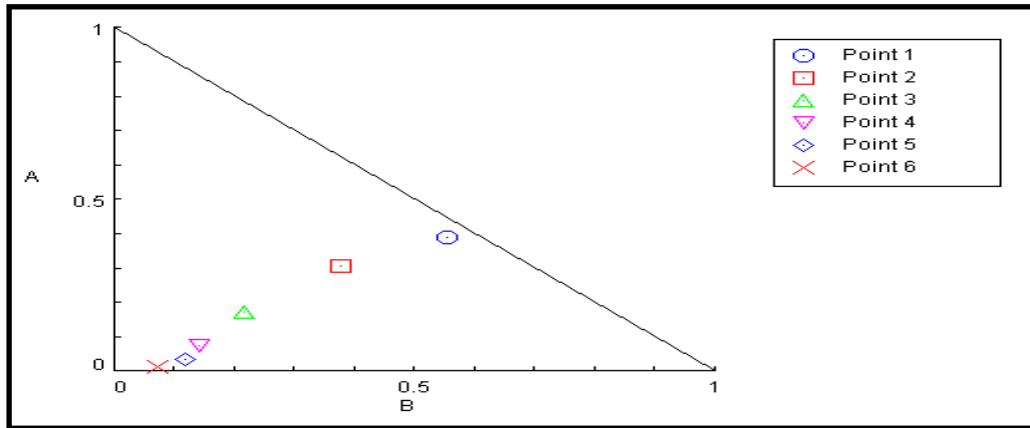


Fig. 8. Isobologram analysis showing the synergistic effect between MV and Ag NPs on Cal cell line

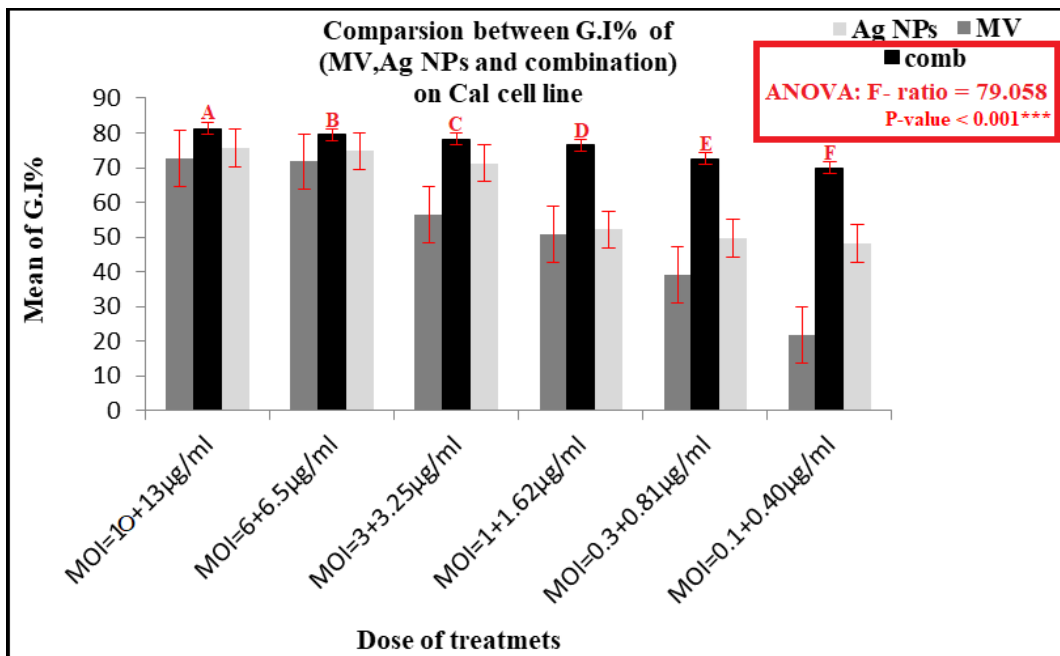


Fig. 9. Comparison between three treatments (MV, Ag NPs alone and MV+ Ag NPs) on Cal-51 cell line. According to Duncan's multiple range comparisons (DMRTs), the mean followed by different letters is significantly different. Means followed by the same letter are not significantly different

differences among the six tested groups ( $p < 0.001$ ) (Fig. 9) shows a comparison of all treatments (MV, AgNPs alone, and MV+AgNP combination) on Cal-51 cells in all six concentrations; the combination treatment has higher growth inhibition rate than MV or AgNPs alone.

*Cytotoxicity of the combined therapy on the normal HBL-100 cell line*

1. **AgNPs:** (Table 3, Fig. 10) demonstrate

that AgNPs have an antagonistic effect with MV on HBL-100 cells after an exposure period of 48 h to all tested concentrations. (Fig. 11) demonstrates that the combination of MV and AgNPs has a weaker effect on the viability of HBL-100 compared with the effect on two cancer cell lines; the high titer of the virus and AgNPs (MOI [10] + 13 µg/ml) revealed an inhibition rate of 21.50% after 48 h of exposure. The comparison between all treatments (MV, AgNPs alone, and AgNPs + MV) on HBL-100 cells showed that the combination treatment has a

Table 3. Antagonistic effect of MV and AgNPs on HBL-100 cells

Point	MV(MOI)	Ag NPs (µg/ml)	G.I%	CI	Effect
1	10	13	0.21	1.35864	Antagonism
2	6	6.5	0.19	1.71472	Antagonism
3	3	3.25	0.15	4.73508	Antagonism
4	1	1.62	0.14	2.61868	Antagonism
5	0.3	0.81	0.13	1.37366	Antagonism
6	0.1	0.40	0.11	1.51705	Antagonism

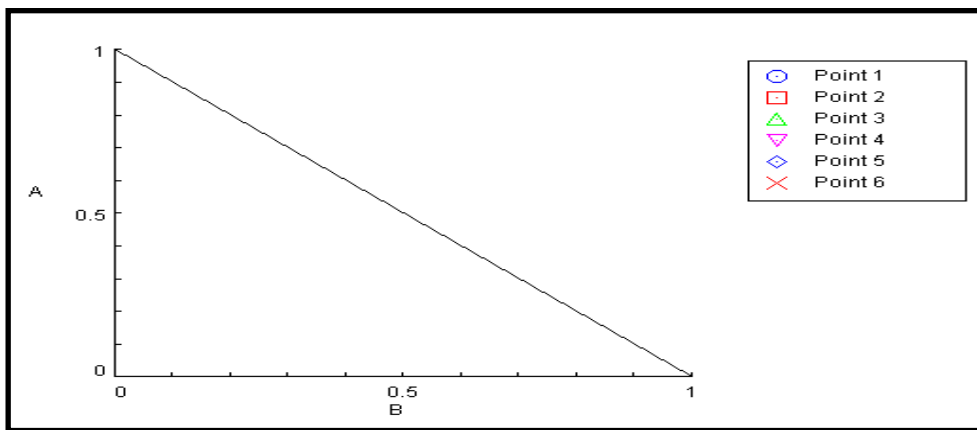


Fig. 10 Isobologram analysis showing the antagonism effect between MV and Ag NPs on HBL-100 cell line at all point.

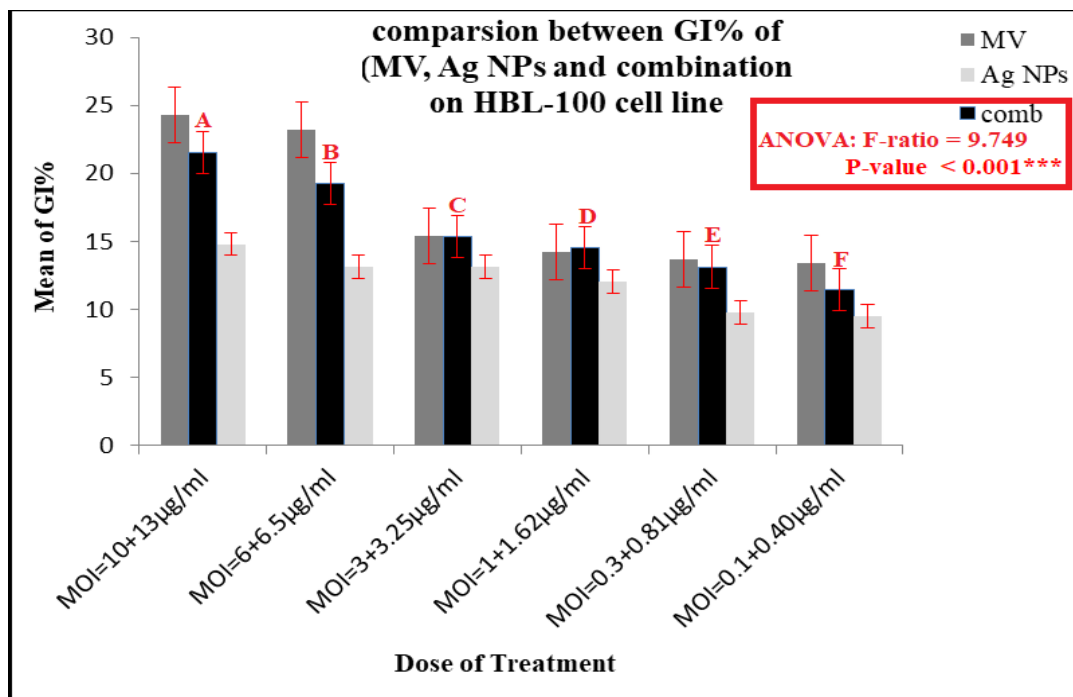


Fig. 11. Comparison between three treatments (MV, Ag NPs alone and MeV+ Ag NPs) at all point on HBL-100 cell line. According to Duncan's multiple range comparisons (DMRTs), the mean followed by different letters is significantly different. Means followed by the same letter are not significantly different

lower effect than MV treatment alone but a higher effect than AgNPs treatment alone at all points (Fig. 11).

## DISCUSSION

The silver nanoparticles showed unique anticancer action against several types of cancer cells. The synthesis approaches used in this study highly affected the cytotoxic activity of the silver nanoparticles (22). The UV/V conducted results are obtained from spectroscopic analysis attributed to the absorption of the SPR of Ag NPs where the silver nanoparticles SPR depended on the reaction between free electrons and the electromagnetic radiation (light) (18). The electrons in the AgNPs moved freely because of the location of the conduction and valence bands, which are located close to each other. The free-electron movement combines both light wave and collective oscillation of AgNPs electrons, consequently increasing the SPR absorption band (23). Thus, a variation in net charge acts as a restoration force, which makes all the electrons in the same phase undergo dipole oscillation (24).

After the synthetization of AgNPs colloidal, all charge is distributed on its surface and in the surrounding area, and these charged the AgNPs which could generate ultimately an ion distribution, as a result of that ,this process will increase the opposite charge on its surface (18). In general, the surface charge of AgNPs can be easily determined by zeta potential analysis; this charge provides a genuine information about all the properties for most particles in suspension. Dispersion stability is improved when the zeta potential value is higher positive than +30 mV or is higher negative than -30 mV because of the strong electrostatic repulsions. A decrease in zeta potential value than (-30 and +30 mV) leads to the formation of aggregate or agglomerate, causing a colloidal instability (25). For this reason, the results of zeta potential analysis of colloidal AgNPs indicates that these particles are more stable in liquid.

AFM considers one kind of scanning probe microscopy (SPM). It explains the resolution on the arrangement of the fragments of a nanoparticle; feeling or touching the surface of a particle on the grid by the mechanical probe is the main mechanism to collect information about imaging, force measurement, and manipulation (26).

In recent research, A higher cytotoxicity

was documented for the smaller sized silver nanoparticles., silver nanoparticles could induce programmed cell death(apoptosis) in the absence of the tumor suppressor p53. traditional cancer therapy usually fails to induce apoptosis in p53-deficient cancer cells. Furthermore, it was proved that nanoparticles of size 5-35 nm prompted cell death via the function affecting(27). the Pgp activity is modulated by AgNPs which enhance the chemotherapeutic efficiency against multi-drug resistant cancer cells; hence, it emphasizes good combinational partners. Currently, the Measles virus is under study as an innovative cancer treatment. The virus replicated in and destroyed cancer cells; it can increase tumor specificity via therapeutic genetically engineered. Prominently, immune responses can be activated against cancer cells by treatment with the measles virus(28). The possibility of virus and silver nano combination to the produced potent outcome as antitumor was evaluated in this study.

First, the oncolytic capacity for Measles Virus (MV) vaccine strain and silver nanoparticles (AgNPs) was measured to destroy breast cancer cells as separate agents. For this purpose, different viral MOIs were used as well as different AgNPs concentrations.

The cytotoxicity assay of MV strain on both types of cell lines after 48 h revealed that the inhibition rates were dosage-dependent; the MOI (10) showed the highest inhibition effect compared with the lowest, which recorded a result of (0.1). MOI. Previous studies anticipated that minimal levels of viruses could not lead to obtained potential virotherapy (29). Many cellular factors play a role in MeV oncolysis sensitivity, like apoptosis and Caspase 3 associated with cancer cell death induced by Me(30) (31).

Moreover, diverse types of breast cancer cell lines needed various MV particles necessary to infect the target cells (typed dependencies). Hence, the kinds and numbers of MV receptors on the target cells will determine the rate of MV infection (32).

By contrast, cytotoxicity occurs when AgNPs destroy the cell membranes; moreover, internalization in the cells generates Reactive Oxygen Species (ROS), which progresses to oxidative stress, thus injuring DNA and proteins, obstructing cell proliferation, and promoting apoptosis (33). As a result, high AgNPs nanoparticle concentration will be adsorbed to

the cell surface or nanoparticle absorption by the cells, or both is lethal to cells. This occurrence leads to the destruction of cell membranes, and AgNPs can induce ROS generation.

Chemically, oxidizing types produce oxidative stress or a significant decrease in the helpfulness of antioxidant resistance; it leads to cell death and can prompt apoptosis through caspase pathways (34).

Under normal conditions, cells regulate ROS levels by balancing **between** generation and elimination of ROS using a scavenging system (35).

Therefore, we combined the virus with the nanoparticles to enhance the effect on cancer cells. This combination produces a synergistic effect on breast cancer cell lines, such as MCF-7 and CAL-51.

## CONCLUSIONS

This study confirms that both silver nanoparticle and MV vaccine strain is targeted the cell lines of breast cancer (MCF-7 and CAL-51) with no lethal effect on the normal cell. The successful formula of AgNPs and MV induced the lethal effect of the cancer cells. Further studies may describe cell death pathways and parameters stimulated by this combination to be an effective recommended **procedure with significant effects of** cancer therapy.

## ABBREVIATIONS

**AFM:** Atomic Force Microscopy  
**CAL-51:** breast cancer cell line (Centre Antoine Lacassagne-51)  
**CIs:** Chou–Talalay combination indices  
**CPE:** cytopathic effects  
**DDW:** double distilled water  
**DMSO:** dimethyl sulfoxide  
**ED50:** median-effect doses  
**GI%:** cell growth inhibition  
**HBL-100:** normal breast epithelial cell line  
**MCF-7:** human breast cancer cell line (Michigan Cancer Foundation)  
**min.:** minute **h:** hour **°C:** degree centigrade  
**mM:** millimole  
**MOI:** multiplicity of infection  
**MTT:** 4,5-dimethylthiazol-2-yl-2,5-diphenyltetrazolium bromide  
**nm:** nanometer  
**PBS:** phosphate buffer saline  
**ROS:** Reactive oxygen species  
**RPMI-1640:** Roswell Park Memorial

## Institute Medium

**SPR:** surface plasmon resonance

**UV/Vis:** Ultraviolet–visible

**VERO-hSLAM:** verda reno - human signaling lymphocytic activation molecule

**µg/ml:** microgram per milliliter

**µm:** micrometer

## ACKNOWLEDGMENT

We are thankful to Mustansiriyah University, Iraqi Center for Cancer and Medical Genetic Research and Department of Chemistry (IBS/UPM) for their technical assistance.

## DECLARATIONS

**Ethics approval and consent to participate**

Not applicable

## CONSENT FOR PUBLICATION

The consent to publish had been taken from each participant in this work.

## AVAILABILITY OF DATA AND MATERIALS

The raw data and materials are available upon request.

## COMPETING INTERESTS

The authors declare that they have no competing interests.

## FUNDING

No funds, grants, or other support was received.

## REFERENCES

1. Bray F, Ferlay J, Soerjomataram I, Siegel RL, Torre LA, Jemal A. Global cancer statistics 2018: GLOBOCAN estimates of incidence and mortality worldwide for 36 cancers in 185 countries. *CA: A Cancer Journal for Clinicians*. 2018;68(6):394-424.
2. O Bryan SM, Mathis JM. Oncolytic Virotherapy for Breast Cancer Treatment. *Curr Gene Ther*. 2018;18(4):192-205.
3. Russell SJ, Peng K-W, Bell JC. Oncolytic virotherapy. *Nat Biotechnol*. 2012;30(7):658-70.
4. Al-Khateeb MM, Muna'am Al-Hilli LA. A study of the prevalence of Estrogen & Progesterone Receptor markers positivity in female breast cancer cases in Al-Yarmouk Teaching Hospital. *Mustansiriya Med J*. 2018;12(2):8.
5. Lech PJ, Russell SJ. Use of attenuated paramyxoviruses for cancer therapy. *Expert Review of Vaccines*. 2010;9(11):1275-302.
6. Kurmi BD, Paliwal R, Paliwal SR. Dual cancer targeting using estrogen functionalized chitosan nanoparticles loaded with doxorubicin-estrone conjugate: A quality by design approach. *International Journal of Biological Macromolecules*. 2020;164:2881-94.
7. Ma Y, Cai F, Li Y, Chen J, Han F, Lin W. A review of the ap-

- plication of nanoparticles in the diagnosis and treatment of chronic kidney disease. *Bioact Mater.* 2020;5(3):732-43.
8. Luo C-H, Shanmugam V, Yeh C-S. Nanoparticle biosynthesis using unicellular and subcellular supports. *NPG Asia Materials.* 2015;7(8):e209-e.
  9. Slepíčka P, Slepíčková Kasálková N, Siegel J, Kolská Z, Švorčík V. *Methods of Gold and Silver Nanoparticles Preparation.* Materials (Basel). 2019;13(1):1.
  10. Salleh A, Naomi R, Utami ND, Mohammad AW, Mahmoudi E, Mustafa N, et al. The Potential of Silver Nanoparticles for Antiviral and Antibacterial Applications: A Mechanism of Action. *Nanomaterials (Basel).* 2020;10(8):1566.
  11. Gargioni C, Borzenkov M, D'Alfonso L, Sperandeo P, Polissi A, Cucca L, et al. Self-Assembled Monolayers of Copper Sulfide Nanoparticles on Glass as Antibacterial Coatings. *Nanomaterials (Basel).* 2020;10(2):352.
  12. Lee PC, Meisel D. Adsorption and surface-enhanced Raman of dyes on silver and gold sols. *The Journal of Physical Chemistry.* 1982;86(17):3391-5.
  13. Šileikaitė A, Prosyčėvas I, Puišo J, Juraitis A, Guobienė A. Analysis of Silver Nanoparticles Produced by Chemical Reduction of Silver Salt Solution. *Mater Sci.* 2006;12(4):1392–1320.
  14. N R Alrawi N, Q Al-ani M, Yaseen NY. CYTOTOXIC EFFECT OF SYNTHESIZED SILVER NANOPARTICLES BY PULSE LASER ABLATION ON BREAST CANCER CELL LINE (AMJ13) FROM IRAQI PATIENT AND NORMAL HUMAN LYMPHOCYTES. *Asian Journal of Pharmaceutical and Clinical Research.* 2018;11(4):375.
  15. Flint J, Racaniello VR, Rall GF, Skalka AM, Hatzioannou T. *Principles of virology, Volume 1: Molecular biology.* John Wiley & Sons; 2020.
  16. Chiang L-C, Chiang W, Chang M-Y, Lin C-C. *In Vitro* Cytotoxic, Antiviral and Immunomodulatory Effects of *Plantago major* and *Plantago asiatica*. *The American Journal of Chinese Medicine.* 2003;31(02):225-34.
  17. Alsaedi IJ, Taqi ZJ, Abdul Hussien AM, Sulaiman GM, Jabir MS. Graphene nanoparticles induces apoptosis in MCF-7 cells through mitochondrial damage and NF-KB pathway. *Materials Research Express.* 2019;6(9):095413.
  18. Le NTT, Nguyen DH, Nguyen NH, Ching YC, Pham Nguyen DY, Ngo CQ, et al. Silver Nanoparticles Ecofriendly Synthesized by *Achyranthes aspera* and *Scoparia dulcis* Leaf Broth as an Effective Fungicide. *Applied Sciences.* 2020;10(7):2505.
  19. Mollick MMR, Bhowmick B, Maity D, Mondal D, Roy I, Sarkar J, et al. Green synthesis of silver nanoparticles-based nanofluids and investigation of their antimicrobial activities. *Microfluidics and Nanofluidics.* 2013;16(3):541-51.
  20. Imran S, Amin N, Arshad MI, Islam MU, Anwar H, Azam A, et al. Structural and optical properties of Cr-substituted Mg-ferrite synthesis by co-precipitation method. *Dig J Nanomater Biostructures.* 2016;11(4):1197–204.
  21. Mohaghegh S, Osouli-Bostanabad K, Nazemiyeh H, Javazadeh Y, Parvizpur A, Barzegar-Jalali M, et al. A comparative study of eco-friendly silver nanoparticles synthesis using *Prunus domestica* plum extract and sodium citrate as reducing agents. *Advanced Powder Technology.* 2020;31(3):1169-80.
  22. Abdel-Fattah WI, W Ali G. On the anti-cancer activities of silver nanoparticles. *Journal of Applied Biotechnology & Bioengineering.* 2018;5(1).
  23. Noginov MA, Zhu G, Bahoura M, Adegoke J, Small C, Ritzo BA, et al. The effect of gain and absorption on surface plasmons in metal nanoparticles. *Applied Physics B.* 2006;86(3):455-60.
  24. Nath S, Chakdar D. Synthesis of CdS and ZnS Quantum Dots and Their Applications in Electronics, *Nanotrends.* 2007;
  25. Mohd Yasin SM, Badruddin IA, Johan MR. Super Stability of Ag Nanoparticle in Crystalline Lamellar (Lc) Liquid Crystal Matrix at Different pH Environment. *Symmetry.* 2019;12(1):31.
  26. Reifengerger R. *Fundamentals of Atomic Force Microscopy: Part I: Foundations.* World Scientific Publishing Company Pte. Limited; 2016.
  27. Souza TAJ, Franchi LP, Rosa LR, da Veiga MAMS, Takahashi CS. Cytotoxicity and genotoxicity of silver nanoparticles of different sizes in CHO-K1 and CHO-XRS5 cell lines. *Mutation Research/Genetic Toxicology and Environmental Mutagenesis.* 2016;795:70-83.
  28. Engeland CE, Ungerechts G. Measles Virus as an Oncolytic Immunotherapy. *Cancers (Basel).* 2021;13(3):544.
  29. Al-Shammari AM, Ismaeel FE, Salih SM, Yaseen NY. Live attenuated measles virus vaccine therapy for locally established malignant glioblastoma tumor cells. *Oncolytic Virother.* 2014;3:57-68.
  30. Boisgerault N, Guillerme J-B, Pouliquen D, Mesel-Lemoine M, Achard C, Combredet C, et al. Natural oncolytic activity of live-attenuated measles virus against human lung and colorectal adenocarcinomas. *Biomed Res Int.* 2013;2013:387362-.
  31. Wang B, Yan X, Guo Q, Li Y, Zhang H, Xie JS, et al. Deficiency of caspase 3 in tumor xenograft impairs therapeutic effect of measles virus Edmoston strain. *Oncotarget.* 2015;6(18):16019-30.
  32. Abdullah SA, Al-Shammari AM, Lateef SA. Attenuated measles vaccine strain have potent oncolytic activity against Iraqi patient derived breast cancer cell line. *Saudi J Biol Sci.* 2020;27(3):865-72.
  33. Nadhe SB, Tawre MS, Agrawal S, Chopade BA, Sarkar D, Pardesi K. Anticancer potential of AgNPs synthesized using *Acinetobacter* sp. and *Curcuma aromatica* against HeLa cell lines: A comparative study. *Journal of Trace Elements in Medicine and Biology.* 2020;62:126630.
  34. Poprac P, Jomova K, Simunkova M, Kollar V, Rhodes CJ, Valko M. Targeting Free Radicals in Oxidative Stress-Related Human Diseases. *Trends in Pharmacological Sciences.* 2017;38(7):592-607.
  35. Dickinson BC, Chang CJ. Chemistry and biology of reactive oxygen species in signaling or stress responses. *Nat Chem Biol.* 2011;7(8):504-11.